A practical graphitic carbon nitride (g-C_3N_4) based fluorescence sensor for the competitive detection of trithiocyanuric acid and mercury ions

Meng Li,[a,b] Bo Wang,[a,b] Xufei An,[a,b] Zhiyong Li,[a,b] Hongtao Zhu,[a,b] Boyang Mao,*[c] David G. Calatayud,*[d] and Tony D. James*[e]

[a]Hebei Key Lab of Power Plant Flue Gas Multi-Pollutants Control, Department of Environmental Science and Engineering, North China Electric Power University, Baoding, 071003, PR China

[b]MOE Key Laboratory of Resources and Environmental Systems Optimization, Ministry of Education, Beijing, 102206, P. R. China

[c]National Graphene Institute, The University of Manchester, Manchester, UK

[d]Department of Electroceramics, Instituto de Ceramica y Vidrio CSIC, Kelsen 5, Campus de Cantoblanco, 28049, Madrid, Spain

[e]Department of Chemistry, University of Bath, Bath, BA2 7AY, UK

Email:t.d.james@bath.ac.uk

Abstract: A fluorescent sensor for the detection of trithiocyanuric acid (TCA) and Hg^{2+} was developed based on competitive interactions: non-covalent stacking between g-C_3N_4 and TCA *vs* coordinative interaction between TCA and Hg^{2+}. Electrostatic simulations were used to evaluate the interactions and help describe the detection mechanism. Moreover, normalized 2D fluorescence contour plots have been used to understand the fluorescence phenomenon. When TCA was added into a g-C_3N_4 nanosheet solution free of Hg^{2+}, TCA interacted with g-C_3N_4 nanosheets *via*

hydrogen bonding and π-π interactions, resulting in fluorescence quenching of the g-C_3N_4 nanosheets. However, upon the addition of Hg^{2+}, the fluorescence of the TCA-g-C_3N_4 nanosheet hybrid system was restored, due to coordination of Hg^{2+} with TCA through the S atoms, breaking the TCA-g-C_3N_4 stacking interaction. Our results provide a new approach for the design of multifunctional nanosensors suitable for the detection of environmental pollutants.

Keywords: fluorescent sensor; graphitic carbon nitride; mercury sensing; dye sensor; functional materials

1. Introduction

With rapid global industrialization, heavy metal ions have polluted the biosphere's water supplies mainly as a result of the disposal of industrial and agricultural waste [1-3]. As a result, organic and/or inorganic pollutants in freshwater systems have become an important environmental issue due to their adverse influence on human health and environmental stability [4-7]. Trithiocyanuric acid (TCA), which is a widely used vulcanizing agent for rubber [8-10], is one of the many contaminants entering the environment. High concentrations of TCA can pose a serious threat to aquatic organisms and human health [11]. Currently, numerous analytical methods have been developed for the detection of TCA, including high-performance liquid chromatography (HPLC) [12], mass spectrometry [13] and electrochemistry. However, the implementation of these detection methods is practically limited by high operational costs, possible secondary contamination and maintenance difficulties. Among the various possible methods to detect TCA, methods using fluorescence have been

demonstrated as an effective alternative due to the simpler equipment requirements, fast response times and lower operating costs [14, 15]. In addition, fluorescence based methods display high sensitivity and selectivity. Nanomaterial-based fluorescent sensors are extremely attractive owing to their intrinsic sensitivity and simplicity [16, 17]. To the best of our knowledge, this is the first report on the detection of TCA using a nanomaterial based fluorescent sensor.

Inorganic pollutants inevitably coexist with organic pollutants in aqueous solutions. Especially mercury ion (Hg^{2+}), one of the most toxic metal ions [18-21], widely exists in the environment and can be converted into methylmercury, a strong neurotoxin that can accumulate in the human body through the food chain resulting in many brain related diseases [22-24]. Significant effort has been devoted to design nanomaterial-based fluorescent sensors for Hg^{2+} detection due to the many advantages including sensitivity, selectivity, versatility and device portability [25-29]. Nevertheless, their widespread implementation has been delayed by the remaining limitations, such as high cost, difficult synthesis and potential chemical toxicity [30]. Moreover, most nanosesnors for Hg^{2+} detection work using a turn-off process, which can result in false signals caused by the existence of other quenchers in real world samples. Therefore, with this research we set out to fabricate a selective turn-on fluorescent sensor for practical applications.

Two-dimensional (2D) nanomaterial based fluorescent sensors are popular due to their low toxicity and excellent optical properties [31, 32]. Among them, graphitic carbon nitride is a chemically and thermally stable metal-free semiconductor [33, 34]. It is the

most stable allotrope of various carbon nitrides under ambient conditions. The framework topology of the previously identified g-C_3N_4 is a defect-rich and N-bridged "poly(tri-s-triazine)" [35].

Our approach uses the coordinative interactions between TCA and Hg^{2+} and non-covalent stacking between g-C_3N_4 and TCA. The fluorescence of g-C_3N_4 nanosheets can be quenched by TCA, due to supramolecular interactions between the aromatic TCA and g-C_3N_4 nanosheets. While, the fluorescence of g-C_3N_4 nanosheets is recovered by the addition of Hg^{2+} since the interaction between Hg^{2+} and TCA results in the removal of TCA from the surface of g-C_3N_4, as shown in **Scheme 1**. The detection system proved to be selective for the detection of TCA and Hg^{2+}. Furthermore, the detection mechanism was evaluated using theoretical calculations. Our results provide a new approach for the design of multifunctional nanosensors based on competitive interactions for the detection of environmental pollutants.

Insert Scheme 1

2. Experimental

2.1 Materials

The reagents were obtained from standard commercial sources and were used as received: isopropyl alcohol (IPA, Tianjin Bei Chen Fang Zheng Reagent, AR, purity ≥ 99.7%), mercury acetate (Shanghai Huadong Reagent Co., Ltd. AR, Purity ⩾ 98%), trithiocyanuric acid (Aladdin Reagent (Shanghai) Co., Ltd. ≥ 95%), potassium chloride (Tianjin Kermel Chemical Reagent Co., Ltd., AR, Purity ≥ 99.5%), zinc

chloride (Tianjin Guangfu Fine Chemical Research Institute, AR, purity ≥ 98.0%), calcium chloride (Tianjin Tianda Chemical Experimental Plant, AR, purity ≥ 96.0%), cobaltous chloride hexahydrate (Tianjin Kermel Chemical Reagent, AR, purity ≥ 99.0%), iron chloride tetrahydrate (Tianjin Guangfu Fine Chemical Research Institute, AR, purity ≥ 99.7%), nickelous chloride (Tianjin Guangfu Fine Chemical Research Institute, AR, purity ≥ 99.0%), magnesium chloride hexahydrate (Tianjin Fuchen Chemical Reagent, AR, purity ≥ 98.0%), sodium hydroxide (Tianjin BeiChen Fang Zheng Reagent, AR, purity ≥ 96.0%), sodium chloride (Tianjin BeiChen Fang Zheng Reagent, AR, purity ≥ 99.5%), Copper chloride (Tianjin Guangfu Fine Chemical Research Institute, AR, purity ≥ 99.0%), Lead chloride（Tianjin Kermel Chemical Reagent, AR, purity ≥ 99.5%）, Iron nitrate nonahydrate (Aladdin Reagent (Shanghai) Co., Ltd. ≥ 98.5%), Silver nitrate（Tianjin Kermel Chemical Reagent, AR, purity ≥ 99.8%）, Cobalt nitrate hexahydrate（Aladdin Reagent (Shanghai) Co., Ltd. ≥ 99%）, Lead nitrate （Tianjin Kermel Chemical Reagent, AR, purity ≥ 99.0%）, Cupric nitrate (Tianjin Fuchen Chemical Reagent, AR, purity ≥ 99.5%), Calcium nitrate (Tianjin Fuchen Chemical Reagent, AR, purity ≥ 99.0%), 2-Mercaptobenzothiazole （Shanghai Macklin Biochemical Co., Ltd. ≥ 98%）, 4-Mercaptobenzoic acid (Shanghai Macklin Biochemical Co., Ltd. ≥ 90%), toluene（Tianjin Kermel Chemical Reagent, AR, purity ≥ 99.5%）, phenol (Tianjin Fuchen Chemical Reagent, AR).

2.2 Instruments

The morphology of the g-C_3N_4 nanosheets was observed using a HitachiS-4800

SEM at the magnification of 2500-100000 times. A JEM-2100 transmission electron microscope (TEM) was employed to observe the morphology and the structure of the sample at an acceleration voltage of 200 kV. The crystalline phases of the prepared samples were characterized *via* X-ray diffraction (XRD, Bruker D8 Advance) under wide-angle (10-900) scanning with a step size of 0.010^{o}. X-ray photoelectron spectroscopy (XPS) was conducted using an ESCALAB 250Xi energy spectrometer with a resolution of 0.48 eV (Ag 3d5/2) and 0.68 eV (C 1s) to investigate the surface chemical composition and valence state of g-C_3N_4, respectively. The obtained UV-vis absorption spectrum was performed on the Beijing Puxi T6 New Century UV-Vis spectrophotometer. Fluorescence detection was performed using Shanghai Lengguang F97 pro fluorescence spectrophotometer.

2.3 Synthesis of g-C_3N_4 nanosheets

Bulk g-C_3N_4 was prepared by direct pyrolysis of melamine in a tube furnace. In detail, 3 g melamine was put in an agate mortar, then put into a ceramic boat, and heated at 550 ^{0}C for 4 h with a heating rate of 5 °C min^{-1} for both of the heating and cooling processes. The obtained yellow powder was the bulk g-C_3N_4. In the next step, ultrathin g-C_3N_4 nanosheets were synthesized by sonication, centrifugation and drying of the bulk g-C_3N_4. Briefly, 0.2 g of bulk g-C_3N_4 powder was dispersed in 200 mL solution with the 1: 1 ratio of water: IPA and the mixture was sonicated for 8 hours. The dispersed solution was placed in a centrifuge tube, centrifuged at 5000 rpm for 5 mins, and the supernatant liquid was freeze-dried for further use.

2.4 Fluorescence detection of TCA and Hg^{2+}

The general detection procedure for TCA was as follows: 200 μL of g-C_3N_4 nanosheets stock solution (0.1 mg mL^{-1}) and different amounts of TCA were sequentially added into a series of 5 mL colorimetric tubes, and finally diluted to 2 mL with water: IPA = 1:1 solution before the fluorescence spectrum was measured.

For the detection of Hg^{2+}, into a series of 5 mL colorimetric tubes, different concentrations of Hg^{2+} were mixed with TCA, then 100 μL of g-C_3N_4 nanosheets stock solution was added into the above solution. The mixture was diluted to 2 mL with water: IPA = 1:1 solution, shaken thoroughly and equilibrated. The reference solution was the same without any ions added.

All fluorescence measurements were performed at room temperature. The pH conditions of the g-C_3N_4 solution in fluorescence titrations were in IPA/ phosphate buffer solution (pH = 5.0, 50/ 50, v/v). The fluorescence intensity was measured with an excition wavelength of 310 nm.

3. Results and discussion

3.1 Characterization of g-C_3N_4

The morphology of g-C_3N_4 nanosheets was characterized by scanning electron microscopy (SEM) and transmission electron microscopy (TEM). From the SEM images (**Figure 1a)**, it can be seen that g-C_3N_4 is a relatively amorphous aggregation and the lamellae flake size are small. TEM images of the g-C_3N_4 (**Figure 1b**) reveals a sheet-like monolayer structure. XRD patterns for bulk g-C_3N_4 and g-C_3N_4 nanosheets confirm the successful exfoliation of bulk g-C_3N_4 (**Figure 1c**). Two peaks at 13° and 27.8° were observed for bulk g-C_3N_4. The peak at 13° derived from

in-planar repeated tri-s-triazine units was indexed to the (100) plane of g-C_3N_4, while the peak centered at 27.8°, a characteristic inter-planar stacking peak of the layered aromatic system, was indexed to the (002) plane in g-C_3N_4. Compared with the bulk g-C_3N_4, the (100) peak in g-C_3N_4 nanosheets disappeared and the (002) peak in g-C_3N_4 nanosheets became weaker, suggesting the successful exfoliation of bulk g-C_3N_4. The binding states of C, N and O of g-C_3N_4 nanosheets were investigated by X-ray photoelectron spectroscopy (XPS) in **Figure d**. The C1s spectrum (**Figure S1a**) could be divided into three peaks. The peak located at 284.6 eV arises from C-C coordination of adventitious carbon. The peak at 288.1 eV corresponds to N-C=N coordination and the peak at 293.8 eV was ascribed to carbonate groups. The N1s spectrum (**Figure S1b**) displayed three peaks at 398.5, 400.4 and 405.4 eV, which could be attributed to the C=N-C, C-N-H and charging effects, respectively. **Figure S1c** shows the O1s spectrum with a binding energy of 531.8 eV, the low oxygen content probably originated from the adsorbed H_2O or CO_2 on to the surface of g-C_3N_4 nanosheets [25].

Insert Figure 1

3.2 Theoretical calculations between g-C_3N_4 and TCA

Theoretical calculations were used to understand the non-covalent interactions between g-C_3N_4 and TCA and help explain the sensing mechanism. The interaction between the g-C_3N_4 fluorescent material and TCA was investigated using electrostatic simulations. First, the structures of both compounds were optimized using MMFF94s

Force Field in Avogadro (v 1.2.0).[36] Then, the electrostatic surface potentials were calculated in MarvinSpace (v 17.21.0), ChemAxon. Different π-π stacking between the fluorescent g-C_3N_4 and TCA were proposed using the Hunter and Sanders (HS) model and calculations of the electrostatic surface potentials (**Figure 2 and S2**). From these results, it was confirmed that TCA can readily attach to the g-C_3N_4 surface by π-π stacking.

Insert Figure 2

3.3 Spectral studies of g-C_3N_4 with TCA and Hg^{2+}

UV-*vis* absorption spectra were used to probe the coordination interaction between Hg^{2+} and TCA. As illustrated in **Figure 3a**, TCA-g-C_3N_4 had similar absorption bands with TCA pristine system, and for the mixture UV absorption peak, there were no obvious peak shift, which indicated that while the TCA was attached on the g-C_3N_4 nanosheet and the week non-covalent π-π stacking between g-C_3N_4 nanosheets and TCA has no significant effect on TCA absorption behaviour. However, upon the addition of Hg^{2+} to the TCA-g-C_3N_4 system solution, the absorption band of TCA has a large blue shift, which proves that the Hg^{2+} ions form coordinative bonds with the sulfur atoms of TCA (**Figure 3b**).

Insert Figure 3

The fluorescence emission properties of g-C_3N_4 in the absence and presence of TCA were examined by 2D fluorescence spectra (**Figure 4a, 4b and Figure S3a**). The

g-C_3N_4 alone exhibits a fluorescence emission when excited at 310 nm and no time dependant changes are observed indicating that the g-C_3N_4 nanosheet is stable. In the presence of TCA, the fluorescence intensity of g-C_3N_4 nanosheets at 436 nm gradually decreases, and the decrease is enhanced with increasing concentrations of TCA, due to formation of non-covalent π-π stacking interactions between the g-C_3N_4 nanosheet and TCA. The detection limit was calculated to be 9.6×10^{-8} M (**Figure S4**). Subsequent addition of Hg^{2+} into the TCA-g-C_3N_4 solution, causes the emission at 436 nm to gradually recover (**Figure 4c** and **Figure S3b**). This reversible fluorescence emission results from the formation of coordination bonds between the Hg^{2+} and TCA, which can remove the TCA from the g-C_3N_4 surface. The effect of pH on the detection of TCA with g-C_3N_4 nanosheets was investigated and changes in pH had little effect on the fluorescence intensity (**Figure S5**). Meanwhile, the fluorescence response of g-C_3N_4 nanosheets towards other aromatic compounds such as 2-mercaptobenzothiazole (2-MPT), 4-mercaptobenzoic acid (4-MBA), toluene, phenol was investigated (**Figure S6**). It can be seen that only the addition of 2-MPT resulted in fluorescence quenching, suggesting the sensor has good selectivity for TCA detection.

The capability of TCA-g-C_3N_4 nanosheet composites for the quantitative detection of Hg^{2+} were determined (**Figure 4c and Figure S3b**). The fluorescence intensity of the g-C_3N_4 nanosheets increases with the addition of Hg^{2+}, suggesting TCA binds to Hg^{2+} and removes it from the g-C_3N_4 nanosheets. The fluorescence does not fully recover to the original intensity, which indicates that some TCA remains

attached to the g-C_3N_4. Furthermore, the fluorescence intensity at 436 nm follows a linear relationship for Hg^{2+} concentrations from 0 to 60 μM, and the detection limit was evaluated to be 6.2×10^{-7} M, indicating that the hybrid is particularly sensitive for the detection of Hg^{2+} (**Figure S7**). The pH dependency for TCA was investigated (**Figure S8a**). It is clear that g-C_3N_4 nanosheets are stable towards TCA over a wide range of pH. Meanwhile, the effect of pH on Hg^{2+} detection was also evaluated (**Figure S8b**). Since the precipitation of $Hg(OH)_2$ occurs at pH ≥ 6. Only acidic pH conditions used for further studies. It was found that pH exerted little effect on the response of g-C_3N_4 nanosheets toward Hg^{2+}, which indicates the potential application of this hybrid system over a wide range of pH.

Insert Figure 4

To evaluate the selectivity of the developed TCA-g-C_3N_4 system for heavy metal ions, a selection of heavy metal ions were evaluated. As shown in **Figure 5a**, only the addition of Hg^{2+} (60 μM) led to an obvious increase in fluorescence intensity of the g-C_3N_4 nanosheets, while negligible changes were observed in the presence of other metal ions (100 μM). The fluorescence titration of g-C_3N_4 nanosheets with different coexisting ions was measured to evaluate the interference of other ions in the detection of Hg^{2+} ions (**Figure 5b)**. It was found that these ions barely had any effect on the fluorescence recovery of the g-C_3N_4 nanosheets, which suggests that the sensor has a high selectivity towards Hg^{2+}. The high selectivity was ascribed to the stronger affinity of thiol-containing ligand for Hg^{2+} compared to other metal ions. Meanwhile,

the effect of the counter ion was determined. Therefore, we evaluated the metal ions with nitrate as the counter ion (**Figure S9)**. It can be seen that the counter ion has little effect on the sensing of Hg^{2+}.

Insert Figure 5

4. Conclusion

In summary, we have designed and fabricated a practical fluorescent sensor for the detection of TCA and Hg^{2+} using g-C_3N_4 nanosheets. Our design principle is promising for the development of nanosensors suitable for the detection of pollutants in wastewater since the fluorescence of the g-C_3N_4 nanosheets was sensitively quenched by TCA (9.6×10^{-8} M for TCA), while the addition of Hg^{2+} to the TCA-g-C_3N_4 nanosheets hybrid led to fluorescence recovery with low detection limits (6.2×10^{-7} M for Hg^{2+}). Furthermore, the detection mechanism was investigated using theoretical calculations to confirm our experimental results. The results reported here provide a new approach for the design of a multifunctional nanosensor for the detection of environmental pollutants. The simplicity of this method makes it suitable for real world applications.

Acknowledgments

The present work is supported by the National Natural Science Foundation of China (No. 21607044), the Natural Science Foundation of Hebei Province (No. B2017502069) and the Fundamental Research Funds for the Central Universities (No. 2018MS113). All data supporting this study are provided as supplementary

information accompanying this paper. T.D.J. wishes to thank the Royal Society for a Wolfson Research Merit Award.

References

[1] Fu F, Wang Q. Removal of heavy metal ions from wastewaters: a review. J Environ Manage. 2011;92(3):407-18.

[2] Li M, Liu Z, Wang HC, Sedgwick AC, Gardiner JE, Bull SD, et al. Dual-function cellulose composites for fluorescence detection and removal of fluoride. Dyes & Pigments. 2018;149:669-75.

[3] Ahmaruzzaman M. Industrial wastes as low-cost potential adsorbents for the treatment of wastewater laden with heavy metals. Adv Colloid Interface Sci. 2011;166(1-2):36-59.

[4] Schwarzenbach RP, Escher BI, Fenner K, Hofstetter TB, Johnson CA, Von GU, et al. The challenge of micropollutants in aquatic systems. Science. 2006;313(5790):1072-7.

[5] Thevenon F, Graham ND, Herbez A, Wildi W, Pot, Eacute J. Spatio-temporal distribution of organic and inorganic pollutants from Lake Geneva (Switzerland) reveals strong interacting effects of sewage treatment plant and eutrophication on microbial abundance. Chemosphere. 2011;84(5):609-17.

[6] Li M, Liu Z, Wang L, James TD, Xiao HN, Zhu W. Glutamic acid-modified cellulose fibrous composite for adsorption of heavy metal ions from single and binary solutions. Mater Chem Front. 2017;1(11):2317-23.

[7] Xiao T, Wang F, Chen Y, Yang X, Wei T, Liu C, et al. Pyrene-based bisboronic sensors for multichannel enantioselective recognition of tartaric acid. Dyes and Pigments. 2019;163:227-31.

[8] Beezer AE, Chudy JC. Elucidation of coordination polymer stoichiometry via thermometric titrimetry: Metal complexes of trithiocyanuric acid. Thermochim Acta. 1973;6(2):231-7.

[9] Hong S, Chen W, Zhang Y, Luo HQ, Li M, Li NB. Investigation of the inhibition effect of trithiocyanuric acid on corrosion of copper in 3.0 wt.% NaCl. Corros Sci. 2013;66(1):308-14.

[10] Fu L, Zhang L, Wang S, Peng J, Zhang G. Silica nanoparticles modified with trithiocyanuric acid as a potential adsorbent forremoval of Ag+ from aqueous solutions. Water Air Soil Pollut. 2017;228(8):273.

[11] Chiu WA, Jinot J, Scott CS, Makris SL, Cooper GS, Dzubow RC, et al. Human health effects of trichloroethylene: Key findings and scientific issues. Environ Health Perspect. 2013;121(3):303-11.

[12] Sergio Gómezalonso, Garcíaromero E. Simultaneous HPLC analysis of biogenic amines, amino acids, and ammonium ion as aminoenone derivatives in wine and beer samples. J Agric Food Chem. 2007;55(3):608-13.

[13] Soga T, Heiger DN. Amino acid analysis by capillary electrophoresis electrospray ionization mass spectrometry. Anal Chem. 2000;72(6):1236-41.

[14] Hirano T, Kikuchi K, Urano Y, Tsunehiko Higuchi A, Nagano T. Highly zinc-selective fluorescent sensor molecules suitable for biological applications. J Am

Chem Soc. 2000;122(49):12399-400.

[15] Zhang X, Ko G, Joung JF, Li M, Jeong Y, Swamy KMK, et al. A naphthoimidazolium-cholesterol derivative as a ratiometric fluorescence based chemosensor for the chiral recognition of carboxylates. Chem Commun. 2018;54(94):13264-7.

[16] Su S, Wu W, Gao J, Lu J, Fan C. Nanomaterials-based sensors for applications in environmental monitoring. J Mater Chem. 2012;22(35):18101-10.

[17] Tao C-L, Chen B, Liu X-G, Zhou L-J, Zhu X-L, Cao J, et al. A highly luminescent entangled metal–organic framework based on pyridine-substituted tetraphenylethene for efficient pesticide detection. Chem Commun. 2017;53(72):9975-8.

[18] Canário J, Vale C, Caetano M. Distribution of monomethylmercury and mercury in surface sediments of the Tagus Estuary (Portugal). Mar Pollut Bull. 2005;50(10):1142-5.

[19] Mauro JBN, Guimarães JRD, Melamed R. Mercury methylation in a tropical macrophyte: influence of abiotic parameters. Appl Organomet Chem. 2010;13(9):631-6.

[20] Xiong C, Li Y, Wang G, Fang L, Zhou S, Yao C, et al. Selective removal of Hg(II) with polyacrylonitrile-2-amino-1,3,4-thiadiazole chelating resin: Batch and column study. Chem Eng J. 2015;259:257-65.

[21] Feng Y, Shao X, Huang K, Tian J, Mei X, Luo Y, et al. Mercury nanoladders: a new method for DNA amplification, signal identification and their application in the

detection of Hg(ii) ions. Chem Commun. 2018;54(58):8036-9.

[22] Duan J, Zhang Y, Yin Y, Li H, Wang J, Zhu L. A novel “on-off-on” fluorescent sensor for 6-thioguanine and Hg 2+ based on g-C 3 N 4 nanosheets. Sens Actuators B-Chem. 2018;257.

[23] Xu D, Wu WD, Qi H-J, Yang R-X, Deng W-Q. Sulfur rich microporous polymer enables rapid and efficient removal of mercury(II) from water. Chemosphere. 2018;196:174-81.

[24] Zhou L, Liu Z, Liu J, Huang Q. Adsorption of Hg(II) from aqueous solution by ethylenediamine-modified magnetic crosslinking chitosan microspheres. Desalination. 2010;258(1):41-7.

[25] Li M, Liu Z, Wang S, Calatayud DG, Zhu WH, James TD, et al. Fluorescence detection and removal of copper from water using a biobased and biodegradable 2D soft material. Chem Commun. 2018;54(2):184.

[26] Gutiérrezdelrío I, Marín L, Fernández J, Millán MÁS, Ferrero FJ, Valledor M, et al. Development of a biosensor protein bullet as a fluorescent method for fast detection of Escherichia coli in drinking water. Plos One. 2018;13(1):e0184277.

[27] Yoon S, Miller EW, He Q, Do PH, Chang CJ. A bright and specific fluorescent sensor for mercury in water, cells, and tissue. Angew Chem Int Ed. 2007;119(35):6778-81.

[28] Lee DH, Kim SY, Hong JI. A fluorescent pyrophosphate sensor with high selectivity over ATP in water. Angew Chem Int Ed. 2004;43(36):4777.

[29] He H, Mortellaro MA, Leiner MJ, Fraatz RJ, Tusa JK. A fluorescent sensor with

high selectivity and sensitivity for potassium in water. J Am Chem Soc. 2003;125(6):1468-9.

[30] Wang J, Li Y, Patel NG, Zhang G, Zhou D, Pang Y. A single molecular probe for multi-analyte (Cr^{3+}, Al^{3+} and Fe^{3+}) detection in aqueous medium and its biological application. Chem Commun. 2014;50(82):12258-61.

[31] Hai-Lin Z, Xiao-Li W, Yi Z, Jia-Yi C, Shanshan L, Xiao-Peng H, et al. Fluorogenic probing of specific recognitions between sugar ligands and glycoprotein receptors on cancer cells by an economic graphene nanocomposite. Adv Mater. 2013;25(30):4097-101.

[32] Song J-X, Tang X-Y, Zhou D-M, Zhang W, James TD, He X-P, et al. A fluorogenic 2D glycosheet for the simultaneous identification of human- and avian-receptor specificity in influenza viruses. Materials Horizons. 2017;4(3):431-6.

[33] Guan W, Sun G, Yin L, Zhang Z, Tian S. Ti_4O_7/g-C_3N_4 Visible Light Photocatalytic Performance on Hypophosphite Oxidation: Effect of Annealing Temperature. Front Chem. 2018;6:37.

[34] Liu Q, Chen T, Guo Y, Zhang Z, Fang X. Ultrathin g-C_3N_4 nanosheets coupled with carbon nanodots as 2D/0D composites for efficient photocatalytic H_2 evolution. Appl Catal, B. 2016;193:248-58.

[35] Zhuang J, Zhang J, Pang J, Wang A, Wang X, Zhu W. Fabrication of pyrimidine/g-C3N4 nanocomposites for efficient photocatalytic activity under visible-light illumination. Dyes and Pigments. 2019;163:634-40.

[36] Hanwell MD, Curtis DE, Lonie DC, Vandermeersch T, Zurek E, Hutchison GR.

Avogadro: an advanced semantic chemical editor, visualization, and analysis platform.

J Cheminformatics. 2012;4(1):17.

Scheme Title and Captions of Figures

Scheme 1. Schematic representation of the sensing process of the g-C_3N_4 nanosheets as a fluorescent sensor for the detection of TCA and Hg^{2+}.

Figure 1. a) SEM image of g-C_3N_4 nanosheets; b) TEM image of g-C_3N_4 nanosheets; c) The Typical XRD patterns of bulk g-C_3N_4 and g-C_3N_4 nanosheets; d) the survey spectrum of g-C_3N_4 nanosheets.

Figure 2. a) Optimized structures of TCA and b) g-C_3N_4 (red denotes areas of relatively high electron density and blue denotes electron deficient areas); c) Proposed stacking arrangements.

Figure 3. a) UV-vis absorption spectrum of g-C_3N_4 nanosheets, g-C_3N_4 nanosheets+TCA, TCA, g-C_3N_4 nanosheets+TCA+Hg^{2+}. The concentrations of g-C_3N_4 nanosheets and TCA and Hg^{2+} were 10 μg mL^{-1}, 45 μM and 60 μM, respectively. b) Schematic representation of possible coordination modes of Hg to TCA.

Figure 4. Normalized 2D fluorescence contour plots recorded for dispersions of: a) g-C_3N_4 solution (0.1 mg mL^{-1}); b) TCA-g-C_3N_4 system upon the addition of TCA (45 μM); c) TCA-g-C_3N_4-Hg system in the presence of Hg^{2+} (60 μM).

Figure 5 a) The relative fluorescence intensity (I/I_0) at 436 nm upon the addition of different metal ions (chloride counter ion); b) The relative fluorescence intensity (I/I_0) at 436 nm after the addition of mixtures of different metal ions with Hg^{2+}. The concentrations of TCA and metal ions were 45 μM and 100 μM, except Hg^{2+} at 60 μM.

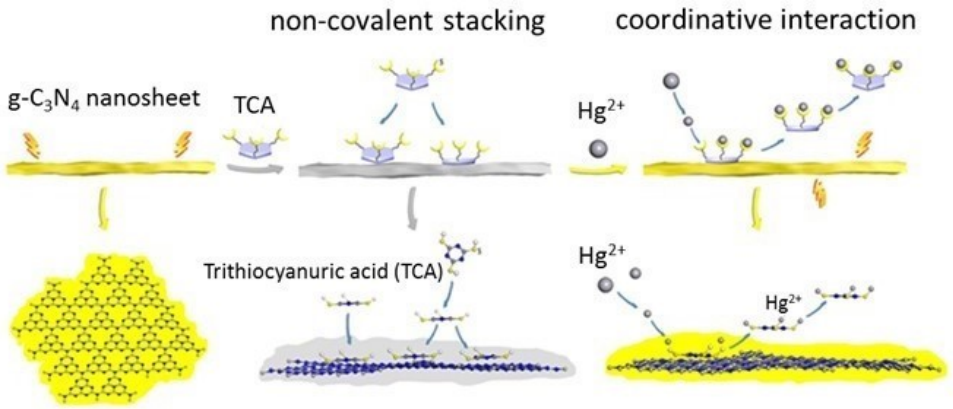

Scheme 1. Schematic representation of the sensing process of the g-C_3N_4 nanosheets as a fluorescent sensor for the detection of TCA and Hg^{2+}.

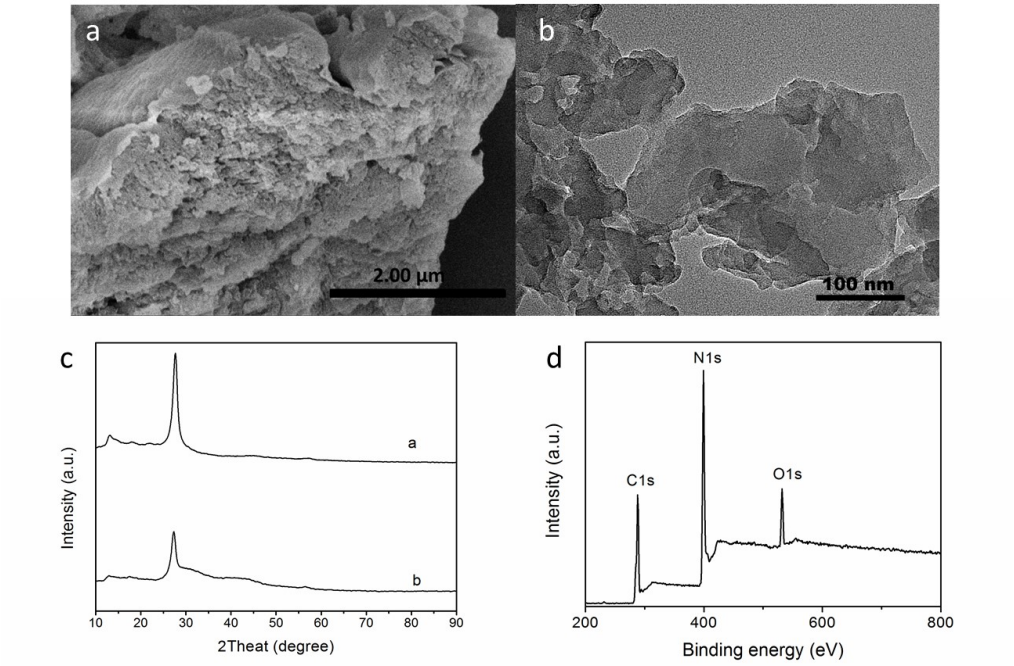

Figure 1. a) SEM image of g-C_3N_4 nanosheets; b) TEM image of g-C_3N_4 nanosheets; c) The Typical XRD patterns of bulk g-C_3N_4 and g-C_3N_4 nanosheets; d) the survey spectrum of g-C_3N_4 nanosheets.

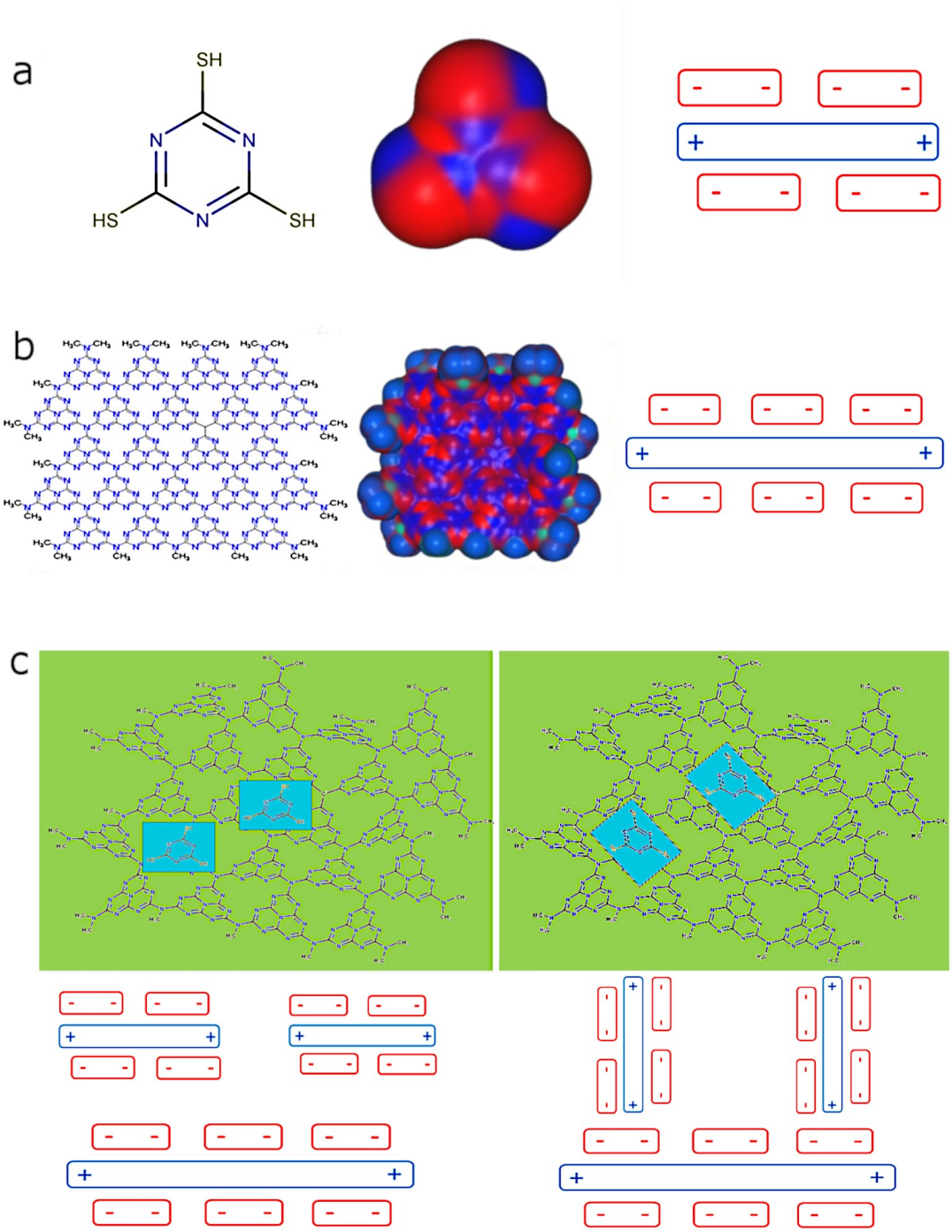

Figure 2. a) Optimized structures of TCA and b) g-C_3N_4 (red denotes areas of relatively high electron density and blue denotes electron deficient areas); c) Proposed stacking arrangements.

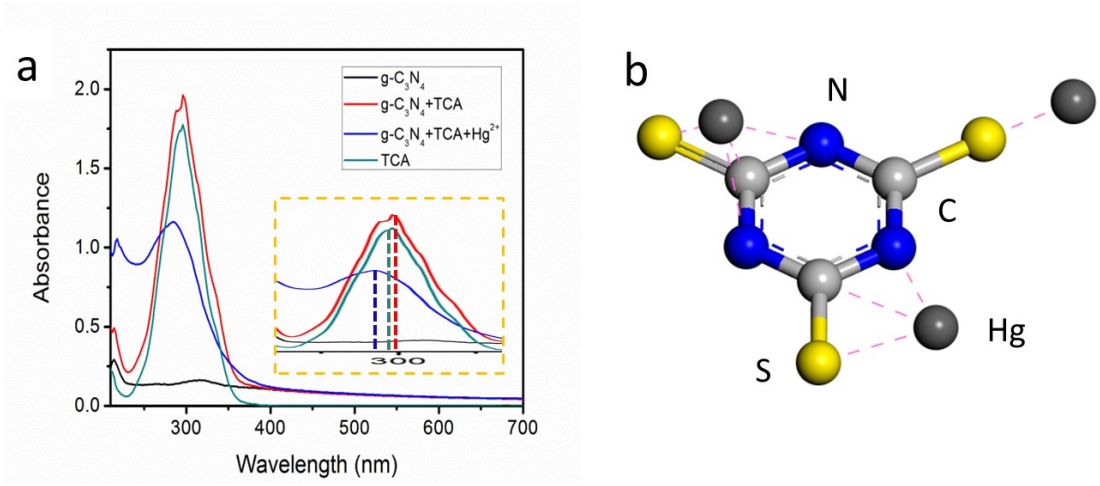

Figure 3. a) UV-vis absorption spectrum of g-C_3N_4 nanosheets, g-C_3N_4 nanosheets+TCA, TCA, g-C_3N_4 nanosheets+TCA+Hg^{2+}. The concentrations of g-C_3N_4 nanosheets and TCA and Hg^{2+} were 10 μg mL^{-1}, 45 μM and 60 μM, respectively. b) Schematic representation of possible coordination modes of Hg to TCA.

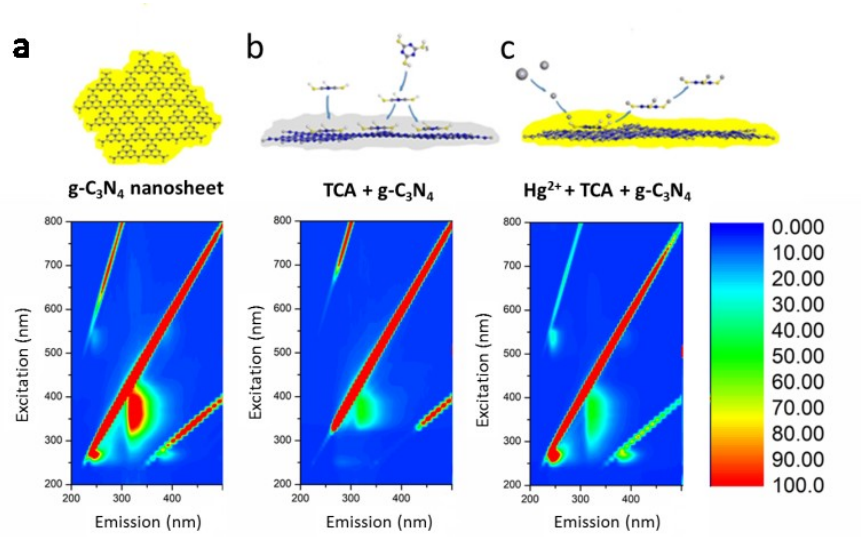

Figure 4. Normalized 2D fluorescence contour plots recorded for dispersions of: a) g-C_3N_4 solution (0.1 mg mL^{-1}); b) TCA-g-C_3N_4 system upon the addition of TCA (45 μM); c) TCA-g-C3N4-Hg system in the presence of Hg^{2+} (60 μM).

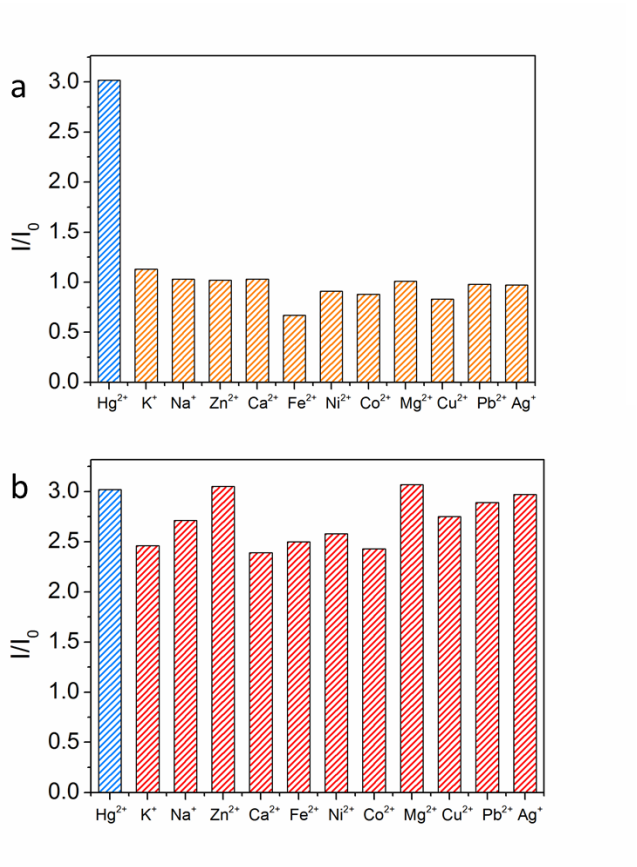

Figure 5. a) The relative fluorescence intensity (I/I_0) at 436 nm upon the addition of different metal ions (chloride counter ion); b) The relative fluorescence intensity (I/I_0) at 436 nm after the addition of mixtures of different metal ions with Hg^{2+}. The concentrations of TCA and metal ions were 45 μM and 100 μM, except Hg^{2+} at 60 μM.